Densities and Phase Equilibria of Aluminum Chloride–Lithium Chloride Melts. 2. Two-Liquid-Phase Region

Ronald A. Carpio, Armand A. Fannin, Jr.,* Fred C. Kibler, Jr., Lowell A. King, and Harald A. Øye†

Frank J. Seiler Research Laboratory (Air Force Systems Command) and Department of Chemistry, United States Air Force Academy, Colorado 80840

The separation into two immiscible liquid phases of $AlCl_3$–LiCl binary melts was studied from ca. 190 to 349 °C. Melt densities and compositions at the point of phase separation were calculated from the expansion of liquids contained in dilatometric tubes. The mole fraction of $AlCl_3$ at phase separation varies from 0.892 at 193.7 °C to 0.839 at 349 °C. Empirical equations are given which express density and mole fraction of $AlCl_3$ at separation as functions of temperature, with overall standard deviations of 0.02 g cm^{-3} and 0.002, respectively. The thermodynamic implications of the phase separation are discussed. A phase diagram is given for the entire $AlCl_3$–LiCl binary system.

Mixtures of $AlCl_3$ and LiCl exhibit a region of liquid–liquid immiscibility at high $AlCl_3$ content. This report describes the temperature–composition–density behavior of $AlCl_3$–LiCl mixtures in the immiscibility region; this is a continuation of our previously reported data on densities of $AlCl_3$–LiCl melts (*1*) and is a companion paper to our study of $AlCl_3$–NaCl immiscibility (*2*).

Experimental Section

Densities were calculated by first measuring the volumes of the two liquid phases and the gas phase, contained in sealed, thick-walled, borosilicate dilatometer tubes. All of the experimental procedures were the same as were reported for the $AlCl_3$–NaCl binary (*2*).

Materials purification and handling, sample preparation and loading, and bath temperature control and measurement were all done as described previously (*1*).

Results and Discussion

Individual tube and sample parameters are given in Table I. Phase volumes are given in Table II at each experimental temperature. The data in Table II were not all taken in the order listed; measurements were made with both ascending and descending temperatures. There was no observable hysteresis in the volumes.

The behavior observed for the $AlCl_3$–LiCl binary system was very similar to that reported earlier for $AlCl_3$–NaCl (*2*), and the data were treated in the same way, except where noted below. For each of the 62 experimental observations for which $t \leq 340$ °C, i.e., up to 9 °C from the critical temperature, the densities of the liquid $AlCl_3$ phase, ρ'', and the density of the $AlCl_3$ gas phase, ρ''', were calculated from Johnson et al. (*3*) using 349 °C as the critical temperature, and ρ' was calculated from eq 1.

$$\rho'v' + \rho''v'' + \rho'''v''' - m_{tot} = 0 \qquad (1)$$

Values of ρ' were then fitted to a straight line, given as eq 2.

$$\rho' = 1.555 - (6.275 \times 10^{-4})t \qquad (2)$$

Table I. Sample Parameters[a]

sample	X^0	v^0, cm^3	m_{AlCl_3}, g	m_{LiCl}, g
I	0.8342	0.90	0.933	0.0590
I	0.8778	0.89	0.664	0.0294
III	0.8997	0.94	0.564	0.0200
IV	0.8998	0.91	0.683	0.0242
V	0.9152	0.90	0.486	0.0143

[a] Estimated uncertainty in mole fraction = ±0.0005. Estimated uncertainty in total volume = ±0.05 cm^3. Estimated uncertainty in mass of $AlCl_3$ = ±0.002 g. Estimated uncertainty in mass of LiCl = ±0.0005 g.

Table II. Liquid-Phase Volumes[a]

t, °C	v', cm^3	v'', cm^3	t, °C	v', cm^3	v'', cm^3
		Sample I			
286.6	0.705	0.035	331.7	0.606	0.195
301.8	0.672	0.083	336.9	0.605	0.208
316.4	0.634	0.141			
		Sample II			
196.9	0.409	0.075	266.1	0.360	0.155
206.5	0.407	0.082	276.2	0.350	0.170
216.0	0.404	0.089	296.4	0.328	0.201
225.9	0.399	0.098	306.4	0.317	0.218
236.5	0.390	0.113	316.2	0.309	0.234
246.5	0.381	0.124	326.4	0.300	0.249
256.3	0.373	0.138	336.0	0.293	0.262
		Sample III			
196.9	0.270	0.148	276.2	0.232	0.211
206.4	0.270	0.150	286.0	0.225	0.220
216.0	0.266	0.157	296.3	0.218	0.228
225.7	0.263	0.163	306.5	0.212	0.236
236.3	0.257	0.172	316.1	0.207	0.241
246.6	0.250	0.182	326.5	0.201	0.242
256.4	0.245	0.191	336.0	0.197	0.236
266.0	0.238	0.202			
		Sample IV			
197.4	0.333	0.174	266.5	0.289	0.259
206.9	0.332	0.180	287.1	0.271	0.294
216.4	0.329	0.189	302.0	0.257	0.320
226.5	0.323	0.200	316.4	0.244	0.351
236.6	0.316	0.213	331.7	0.235	0.383
246.9	0.306	0.229	336.9	0.233	0.401
256.8	0.298	0.243			
		Sample V			
196.9	0.188	0.170	276.2	0.162	0.213
206.5	0.186	0.173	285.8	0.158	0.218
216.0	0.178	0.184	296.4	0.154	0.223
225.9	0.178	0.187	306.4	0.150	0.225
236.5	0.179	0.188	316.2	0.147	0.228
246.5	0.175	0.194	326.4	0.144	0.221
256.3	0.171	0.200	336.0	0.141	0.204
266.1	0.167	0.207			

[a] Estimated uncertainty in temperature = ±0.5 °C. Estimated uncertainty in phase volumes = ±0.005 cm^3.

This equation gives the density along the immiscibility line which is only dependent on temperature. The standard deviation in ρ' was 0.02 g cm^{-3}. Plots of v' vs. t show no noticeable deviations as they pass 340 °C to the critical temperature. It appears that one can safely use eq 2 in the region from 340

† Permanent address: Institutt for Uorganisk Kjemi, Norges Tekniske Høgskole, Universitetet i Trondheim, 7034 Trondheim—NTH, Norway.

Table III. Thermodynamic Properties of Al_2Cl_6

	ΔH_{T_M},[a] kJ mol^{-1}	$\Delta C_{p(T_M)}$,[a] J mol^{-1} K^{-1}	$\Delta H_{T_{crit}}$,[a] kJ mol^{-1}	$C''_{p(T_M)}(Al_2Cl_6) - C'_p(Al_2Cl_6)$, J mol^{-1} K^{-1}
$AlCl_3$ (6)	39.7	−80.3	27.7[b]	
$AlCl_3$-LiCl	40.5 ± 0.8	−52 ± 1[c]	32.4	28.3
$AlCl_3$-NaCl (2)	40.2 ± 0.2	−47.2 ± 0.4[c]	32.9	33.1

[a] These quantities refer to the vaporization to an ideal gas. [b] This is a value extrapolated from lower temperatures by vaporization to an ideal gas. The real value of $\Delta H_{T_{crit}}$ is, of course, zero. [c] Assumed constant over the whole temperature range.

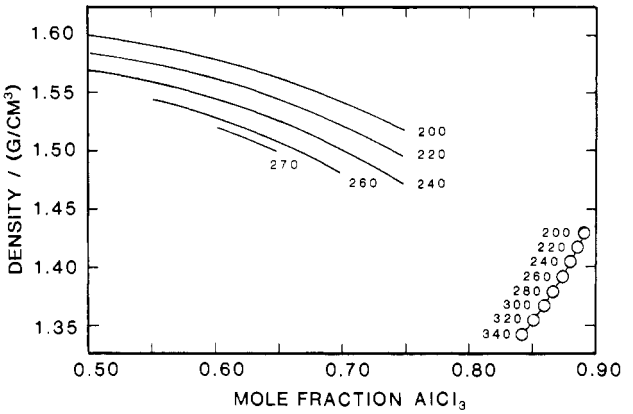

Figure 1. Densities of the single-liquid-phase region of the $AlCl_3$–LiCl binary system: temperatures of isotherms and points in °C; solid lines on left from ref *1*; (O) calculated from eq 2 and 4.

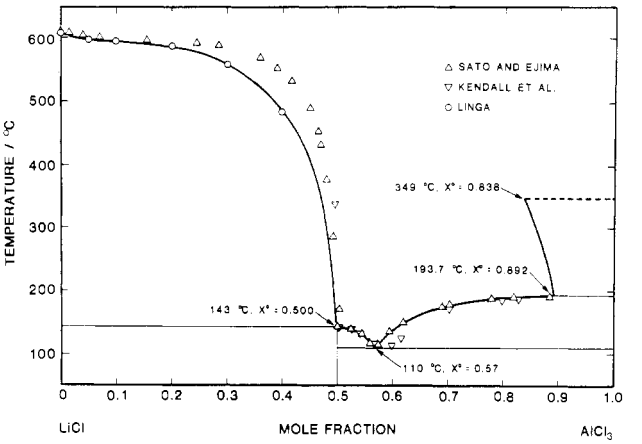

Figure 2. Phase diagram of the $AlCl_3$–LiCl binary system: (▽) data of Kendall et al. (*7*); (△) Sato and Ejima (*8*); (O) Linga (*9*); immiscibility line from eq 4; X^0, t for limits of liquid immiscibility line from present work and ref *10*; X^0, t for monotectic and eutectic from ref *8*.

to 349 °C. In Figure 1, densities are given for the complete single-liquid region at selected temperatures. The points on the right represent the mole fractions at which phase separation occurs. They were calculated from eq 2 and 4 (see below). No density measurements are available for the region between $X' = 0.75$ and phase separation.

The mole fraction of the LiCl-containing phase, X', was calculated at each of the 62 experimental points for which $t \leq 340$ °C by first determining the weight fraction y' from eq 3,

$$y'\rho'v' + y''\rho''v'' + \rho'''v''' - m_{AlCl_3} = 0 \quad (3)$$

with the assumption that $y'' = 1.000$. (Equation 1 can be solved simultaneously for all three phase densities, and from these values y' and y'' can be simultaneously obtained from eq 3. For five selected temperatures from 226 to 346 °C, inclusive, the calculated mean y'' was greater than 0.995.) These mole fractions were fitted to a quadratic polynomial, given as eq 4. The standard deviation in X' was 0.002. As with eq 2,

$$X' = 0.90496 + (9.5223 \times 10^{-5})t - (8.2622 \times 10^{-7})t^2 \quad (4)$$

it appears that eq 4 can be extrapolated safely to the critical temperature of $AlCl_3$.

The present data may be thermodynamically evaluated in much the same way as was done for the $AlCl_3$–NaCl immiscibility data (*2*). In that study we presented the equation

$$\frac{(\Delta H_{T_M} - \Delta C_p T_M)(T - T_M)}{RTT_M} + \frac{\Delta C_p}{R} \ln (T/T_M) = \ln (P''_T/P''_{T_M}) - \ln (a_{T_M}/a'_{T_M}) \quad (5)$$

where ΔH_T and ΔC_p refer to the vaporization process

$$2AlCl_3(l)\ (\text{in } AlCl_3\text{–LiCl}) = Al_2Cl_6(g) \quad (6)$$

and the remaining symbols are defined in the text and the Glossary and in Figure 5 of ref *2*.

From a species model (*4*), based on vapor pressure data (*5*), we found the activity of Al_2Cl_6 was given by

$$a_{T_M} = a'_{T_M}[1 + 3.0(X'_T - X'_{T_M})] \quad (7)$$

When pure liquid $AlCl_3$ is chosen as the standard state, $a_{T_M} = 1$. The factor $\ln (P''_T/P''_{T_M})$ can be calculated from the JANAF Tables (*6*). The values X'_{T_M}, ΔH_{T_M}, and ΔC_p were then determined from a least-squares fit of the experimental data using eq 5. This yielded the values $X'_{T_M} = 0.8917$, $\Delta H_{T_M} = 40.5 \pm 0.8$ kJ mol^{-1}, and $\Delta C_p = -52 \pm 1$ J mol^{-1} K^{-1}.

When eq 5 was rearranged to give X'_T as a function of T, with the fit values of ΔH, ΔC_p, and X'_{T_M} substituted in, a plot of X'_T vs. T was virtually superimposable upon a plot of eq 4.

Figure 2 shows for the first time the complete phase diagram for the binary system $AlCl_3$–LiCl. The liquid–liquid immiscibility line, eq 4 or 5, is the phase boundary when the system is subject to its own vapor pressure. This reaches values considerably higher than 1 atm.

The locus of eq 4 or 5 on an X, t diagram moves away from the $AlCl_3$ axis with increasing temperature even more sharply than for the $AlCl_3$–NaCl system and does not describe the typical dome generally observed for liquid–liquid immiscibility. The curvature is also opposite to what usually is found. The same behavior was noted for the $AlCl_3$–NaCl binary melt. Similarly, the negative slope of the X', t curve can have unexpected implications in applications where one is working with $AlCl_3$–LiCl mixtures near the demixing composition. A temperature rise of a sufficiently $AlCl_3$-rich melt could cause a phase separation which may not reequilibrate into a single phase upon cooling. It is kinetically difficult to transfer $AlCl_3(l)$ into $AlCl_3$–LiCl without physically agitating the interface.

The liquidus line on the LiCl-rich side of Figure 2 is drawn through the data of Linga (*9*, *11*) rather than through the data of Sato and Ejima (*8*). The former data were obtained by differential thermal analysis (DTA) measurements in sealed quartz capillaries (*9*) and, independently, by calculation from vapor pressure measurements (*11*). Sato and Ejima visually observed the disappearance of a solid phase upon heating. They determined their monotectic temperature by DTA.

Finally, we might comment on implications of the immiscibility gap in the $AlCl_3$–LiCl and $AlCl_3$–NaCl systems. Table III gives

the thermodynamic properties of Al_2Cl_6 in pure $AlCl_3$ and in the alkali chloride containing phases in equilibrium with $AlCl_3$. The notable feature is that the enthalpies of vaporization of Al_2Cl_6(gas) are the same within the limits of uncertainty for all three phases at the melting point of $AlCl_3$, while ΔC_p values for the vaporization are nearly equal for the alkali chloride containing phases and less negative than for pure $AlCl_3$(l). This confirms the previous statement (*2*) that the "anomalous" slope of the immiscibility line is most likely attributed to the properties of the $AlCl_3$ phase. That is, $C''_p(Al_2Cl_6)$ in the $AlCl_3$ phase is larger than the partial molar $C'_p(Al_2Cl_6)$ in the ionic mixtures (Table III, last column) due to a greater decrease of attractive forces with temperature in the covalent, near-critical $AlCl_3$ phase. Even though $C'_p(Al_2Cl_6)$ is about equal for the two alkali chloride systems, $C'_p(Al_2Cl_6)$ for the most ionic system, $AlCl_3$–NaCl, as expected deviates the most from that of $AlCl_3$(l) (Table III). The immiscibility gap for the $AlCl_3$–LiCl system (Figure 2) is less than for $AlCl_3$–NaCl, but the variation in immiscibility with temperature is larger for the $AlCl_3$–LiCl system. This is also a simple consequence of a more ideal behavior of the more covalent $AlCl_3$–LiCl mixture.

Safety

Appropriate precautions should be taken for the containment of liquids considerably above their normal boiling points in glass vessels. An especially dangerous situation can occur when $(\rho'' + \rho''')/2 > \rho_{crit}$. The gaseous phase will disappear above a certain temperature and the expansion of liquid $AlCl_3$ will eventually result in rupture of the tube.

Glossary

a	activity of Al_2Cl_6
C_p	heat capacity at constant pressure, J mol^{-1} K^{-1}
H	enthalpy, kJ mol^{-1}
m	mass, g
P	ideal gas pressure of Al_2Cl_6
t, T	temperature, °C and K, respectively
T_M	triple-point temperature of $AlCl_3$, 466.85 K
v	volume, cm^3
X	mole fraction of $AlCl_3$, $AlCl_3$–LiCl scale
y	weight fraction of $AlCl_3$, $AlCl_3$–LiCl scale
ρ	density, g cm^{-3}
0, ′, ″, ‴	superscripts denoting overall sample, $AlCl_3$–LiCl phase, $AlCl_3$(l) phase, and $AlCl_3$(g) phase, respectively

Registry No. $AlCl_3$, 7446-70-0; LiCl, 7447-41-8.

Literature Cited

(1) Carpio, R. A.; King, L. A.; Fannin, A. A., Jr. *J. Chem. Eng. Data* **1979**, *24*, 22.
(2) Fannin, A. A., Jr.; King, L. A.; Seegmiller, D. W.; Øye, H. A. *J. Chem. Eng. Data* **1982**, *27*, 114.
(3) Johnson, J. W.; Cubicciotti, D.; Silva, W. J. *High Temp. Sci.* **1971**, *3*, 523.
(4) Øye, H. A., Universitetet i Trondheim, Trondheim, Norway, unpublished data, 1981.
(5) Bunting, R.; Carpio, R. A.; Fannin, A. A., Jr.; King, L. A.; Øye, H. A., United States Air Force Academy, unpublished data, 1981.
(6) "JANAF Thermochemical Tables", 2nd ed.; *Natl. Stand. Ref. Data Ser. (U.S., Natl. Bur. Stand.)* **1971**, *No. 37*.
(7) Kendall, J.; Crittenden, E. D.; Miller, H. K. *J. Am. Chem. Soc.* **1923**, *45*, 963.
(8) Sato, Y.; Ejima, T. *Nippon Kinzoku Gakkaishi* **1978**, *42*, 905.
(9) Linga, H. Thesis No. 36, Institutt for Uorganisk Kjemi, Norges Tekniske Høgskole, Trondheim, Norway, 1979.
(10) Viola, J. T.; Seegmiller, D. W.; Fannin, A. A., Jr.; King, L. A. *J. Chem. Eng. Data* **1977**, *22*, 367.
(11) Linga, H.; Motzfeldt, K.; Øye, H. A. *Ber. Bunsenges. Phys. Chem.* **1978**, *82*, 568.

Received for review February 10, 1982. Accepted August 13, 1982.

Isothermal Vapor–Liquid Equilibria for Six Binary Mixtures

Tatsuhiko Ohta, Tomoyuki Kinoshita, and Isamu Nagata*

Department of Chemical Engineering, Kanazawa University, Kanazawa 920, Japan

Isothermal vapor–liquid equilibrium data were reported for six binary systems: ethyl formate–carbon tetrachloride, ethyl formate–chlorobenzene, ethyl formate–toluene, ethyl formate–acetonitrile, chloroform–toluene, and acetonitrile–1-propanol. The experimental data were well correlated with the UNIQUAC equation (Anderson and Prausnitz's modification). The UNIFAC group-interaction parameters were obtained for the groups, ACH/HCOO, $ACCH_2$/HCOO, CCl_4/HCOO, ACCl/HCOO, CCN/HCOO, $ACCH_2$/CCl_3, CCOH/CCN, and OH/CCN.

Introduction

Isothermal vapor–liquid equilibrium data were measured for the following binary systems: ethyl formate–carbon tetrachloride at 318.15 K, ethyl formate–chlorobenzene at 323.15 K, ethyl formate–toluene at 318.15 K, ethyl formate–acetonitrile at 323.15 K, chloroform–toluene at 318.15 K, and acetonitrile–1-propanol at 328.15 K. The experimental results were correlated with Anderson and Prausnitz's UNIQUAC equation (*1*, *12*). The UNIFAC group-interaction parameters for the groups ACH/HCOO, $ACCH_2$/HCOO, CCl_4/HCOO, ACCl/HCOO, CCN/HCOO, $ACCH_2$/CCl_3, CCOH/CCN, and OH/CCN were obtained to extend the range of applicability of the UNIFAC method (*14*).

Table I. Densities and Refractive Indices of Compounds at 298.15 K

	density, g/cm^3		refractive index	
compd	exptl	lit.[a]	exptl	lit.[a]
ethyl formate	0.9201[b]		1.359 98[b]	1.359 94[b]
carbon tetrachloride	1.5845	1.584 39	1.457 2	1.457 39
chlorobenzene	1.1010	1.101 12[c]	1.521 7	1.521 9[c]
toluene	0.8622	0.862 31	1.494 1	1.494 13
acetonitrile	0.7767	0.776 6	1.341 6	1.341 63
chloroform	1.4797	1.479 88	1.442 9	1.442 93
1-propanol	0.7995	0.799 75	1.383 5	1.383 70

[a] Reference *13*. [b] At 293.15 K. [c] Reference *16*.

Experimental Procedures

Materials. Guaranteed reagent-grade materials excluding 1-propanol and chloroform were used for experimental work without further purification. Chemically pure grade 1-propanol

0021-9568/83/1728-0036$01.50/0